A Dual-Band Decoupling Technique for MIMO Antenna Systems Using Composite Capacitor Circuits

Jiangwei Sui, *Member, IEEE*, Yi-Feng Cheng, *Member, IEEE*, Xiaohu Fang, *Senior Member, IEEE*, Du Li, Xiangwei Zhu, and Xuelin Yuan

***Abstract*—This paper presents a dual-band antenna decoupling technique with independent control using composite capacitors. Due to the inherent frequency-selective characteristic of the decoupling structure, the decoupling in one band has almost no effect on that in the other band, so the decoupling in the two bands can be independently controlled simply by providing two different desired capacitances, which is achieved using the proposed composite capacitors. An equivalent circuit is presented to reveal the mechanism of the decoupling and frequency-selective characteristics. Two demonstrative examples using proposed composite capacitor circuits are extensively studied by simulation and measurement. The results show that with the proposed decoupling scheme, not only the isolation but also the performance of the total efficiencies and the envelope correlation coefficients are all improved. Benefiting from the composite capacitors, the total footprint of the dual-band decoupling structure is only 5×3 mm^2, which is extremely compact compared with the existing methods.**

***Index Terms*—Antenna decoupling, composite capacitor circuits, dual-band, frequency-selective, independent control, mutual coupling.**

I. Introduction

To satisfy the increasing demands for higher data rates, the multi-band multi-input and multi-output (MIMO) scheme has become one core air-interface technique. However, due to the compact available space for antennas, mutual couplings inevitably exist among antenna elements, which will significantly deteriorate the system's data throughput [1], [2].

Various techniques have been proposed to deal with antenna mutual couplings in single-band scenarios, such as utilizing neutralization lines [3], parasitic elements [4], lumped decoupling elements [5], special ground structure [6], [7], orthogonal modes [8], just name a few. To solve the dual-band mutual coupling problem, many efforts also have been devoted. An effective method is to use a special ground structure, such as a T-shaped slot [9], and a spiral line [10]. But one challenge is that the size of these ground structures is somewhat bulky. Another category of dual-band decoupling technique is to design a dual-band decoupling circuit or a decoupling surface, which can be realized using lumped elements [11], metasurface structure [12], microstrip lines [13] – [15], microstrip stubs [16], and parallel lines [17]. Although these methods can provide systematic design guidelines from the circuit derivation aspect, they usually occupy a large size to implement the decoupling circuits.

Recently, a new decoupling technique using decoupling capacitors is proposed to mitigate the mutual coupling of two single-band antennas by the authors [18], [19]. In this paper, the inherent frequency-selective decoupling characteristic of this method is studied for the first time. Based on this inherent frequency-selective decoupling characteristic, an independently-controlled dual-band decoupling can be achieved by providing two desired capacitances at the two bands, which is realized using the proposed composite capacitor circuit. Compared with the prior dual-band decoupling methods, it presents three distinct features:

1) the decoupling in the two bands is independent of each other;

2) the antenna elements are not required to be physically connected with the decoupling structure; and

3) the occupied size of the decoupling structure is extremely small.

II. Decoupling Scheme and Mechanism

A. Decoupling Scheme

Fig. 1 shows the evolution diagram of the proposed decoupling method. At first, one group of capacitors, C_1, is introduced on the outstretched stubs from the ground to decouple two single-band antennas, as has been discussed in

Manuscript received xxxx xx, 2023; accepted xxxx. This work was supported in part by the National Key R&D Program of China under Grant 2021YFA0716500, in part by Science, Technology and Innovation Commission of Shenzhen Municipality under grant RCBS20210706092348050, and in part by the National Natural Science Foundation of China under Grant 62201625, 62001525, and 62201183. (*Corresponding author: Xuelin Yuan.*)

Jiangwei Sui, Du Li, Xiangwei Zhu, and Xuelin Yuan are with the School of Electronics and Communication Engineering and Shenzhen Key Laboratory of Navigation and Communication Integration, Shenzhen Campus of Sun Yat-sen University, Shenzhen 518000, China (e-mail: suijw@mail.sysu.edu.cn; lidu5@mail.sysu.edu.cn; zhuxw666@mail.sysu.edu.cn; yuanxlin3@mail.sysu.edu.cn).

Yi-Feng Cheng is with the School of Electronics and Information, Hangzhou Dianzi University, Hangzhou 310018, China (e-mail: chengyifeng2013@gmail.com).

Xiaohu Fang is with the School of Micro-electronics, Southern University of Science and Technology, Shenzhen 518000, China (email: fangxh@sustech.edu.cn).

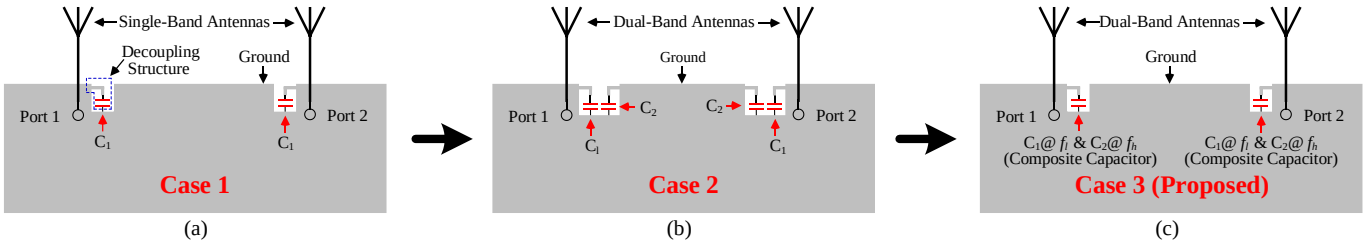

Fig. 1. Evolution diagram of the proposed independently-controlled dual-band decoupling scheme using composite capacitors. (a) Case 1: single-band decoupling. (b) Case 2: Dual-band decoupling using two separate decoupling capacitors. (c) Case 3 (Proposed): Dual-band decoupling using composite capacitors.

[18]. In Case 2, two groups of capacitors, two C_1 and two C_2, can be introduced on four corresponding stubs, as is shown in Fig. 1(b). And the decoupling in the low band is just controlled by adjusting the capacitances of C_1, while the decoupling in the high band is controlled by tuning C_2. Moreover, as is shown in Fig. 1(c), to further reduce the footprint of the whole antenna design, the composite capacitor is proposed to achieve the two desired capacitances in the two bands, C_1 at f_l and C_2 at f_h, respectively.

B. Frequency Selectivity

As the prior art of a single-band decoupling scheme shows in Fig. 1(a), a small rectangle is cut from the ground, and a proper capacitor is inserted between the ground and a short outstretched stub. The intuition tells us that the loading capacitor and the connected stub together with some other parasitic effect constitute a series resonant circuit. To describe this attribute more clearly, an equivalent circuit for decoupling two antennas using decoupling capacitors is depicted in Fig. 2, in which the original coupling consists of a capacitive coupling and an inductive coupling.

Without loss of generality, a validation example using the decoupling scheme shown in Fig. 1(b) is used to study the working mechanism. As the antenna geometry shown in Fig. 3, two dual-band inverted-F antennas (IFAs) working in two bands, 1.8 – 1.88 GHz (5G N3 band) and 3.4 – 3.6 GHz (5G N78 band) are mounted along the same edge of the ground plane formed on one side of an FR4 substrate with a thickness of 1.6 mm, permittivity of 4.3 and loss tangent of 0.02. Compared with the coupled and decoupled cases, the only difference lies in the cut and capacitors on the ground plane for decoupling. By fitting the simulated results of the EM and circuit models of the coupled case, the element values of the equivalent circuit can be obtained, as listed in Table I. Figs. 4(a) and 4(c) depict the comparison of the circuit and EM simulated results in the low band and high band of the coupled IFAs, respectively, showing good agreement. And for the decoupled one, the extra coupled series-resonant decoupling circuit is introduced, as also listed in Table I. Figs. 4(b) and 4(d) show the S-parameters of the decoupled cases in the low and high bands, respectively. The phase results also show similar agreement and are omitted here for brevity.

To study the frequency selectivity, the S-parameters of the circuit model for the coupled and decoupled cases are compared in Fig. 5. In the low band (Fig. 5(a)), the RLC decoupling circuit decouples the two IFAs within the desired band of 1.8 to 1.88 GHz, while leaving the other bands almost unaffected. In the high band (Fig. 5(b)), the RLC decoupling

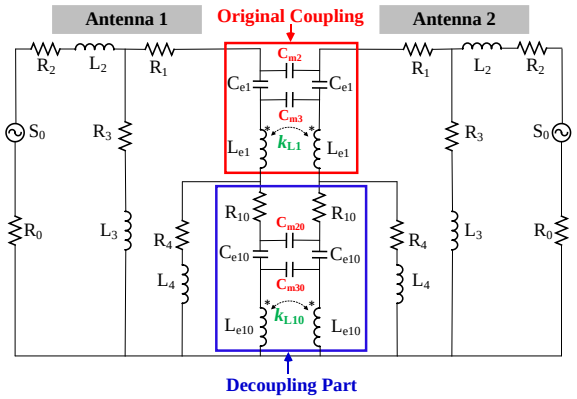

Fig. 2. An equivalent circuit of decoupling two MIMO antennas using decoupling capacitor scheme.

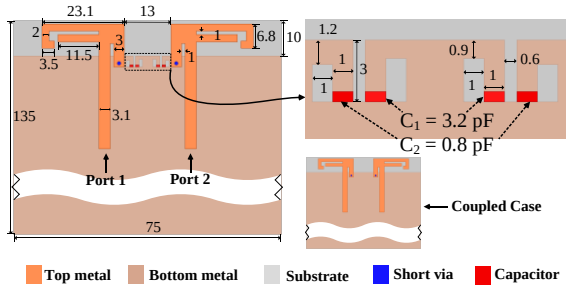

Fig. 3. The geometry of the demonstrative example of two dual-band MIMO antennas using separate capacitors.

circuit only affects a band of 3.2 to 3.8 GHz, also presenting an inherent frequency selectivity. To further justify the circuit model, the reactance of the decoupling circuit in Fig. 2 is also studied for both the low and high bands. It is found that the decoupling circuit presents a low reactance in the desired band while a high reactance in other bands, indicating a natural frequency selectivity.

C. Composite Capacitors

To make the decoupling structure more compact, a composite capacitor is proposed, as has been shown in Fig. 1(c). And to construct the desired composite capacitors, the required capacitor value in the two bands should be discussed first. As has been discussed in the above Part B, the introduced capacitor and the outstretched stub constitute an LC series resonant circuit that resonates in the working band. Therefore, for one certain outstretched stub, whose equivalent inductance is a constant, the required capacitor value in the low band is higher than that in the high band, meaning that C_1 is larger than C_2. Based on this rule, two composite circuits composed of three elements are proposed in Fig. 6.

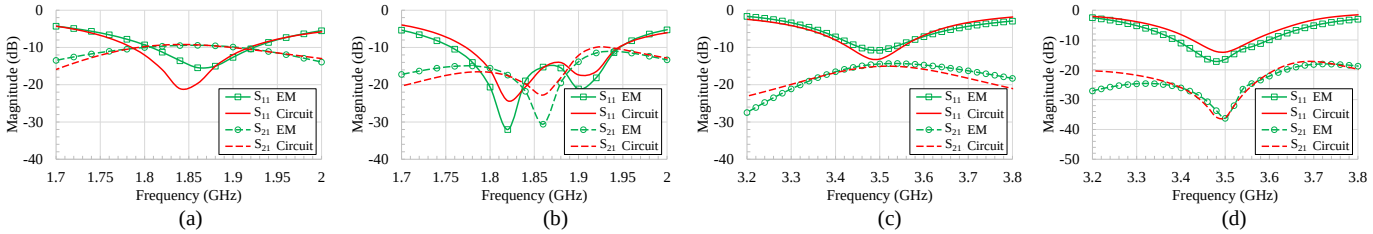

Fig. 4. Magnitude of circuit and EM simulated results. (a) Coupled case in the low band. (b) Decoupled case in the low band. (c) Coupled case in the high band. (d) Decoupled case in the high band.

TABLE I
ELEMENT VALUES OF THE EQUIVALENT CIRCUIT IN THE TWO BANDS
(Units for R, L, and C are Ω, nH and pF.)

	Decoupled Antennas											
	Coupled Antennas								Decoupling Part			
Low band	R_1	0.02	R_2	13.2	L_3	1.28	C_{m2}	1.81	R_{10}	2	C_{m20}	0
	L_{e1}	0.4	L_2	4.56	R_4	2.12	C_{m3}	10	L_{e10}	2.5	C_{m30}	3
	C_{e1}	4.4	R_3	0.02	L_4	0.32	k_{L1}	0	C_{e10}	3.2	k_{L10}	0.69
High band	R_1	0.02	R_2	0.03	L_3	4.85	C_{m2}	0.08	R_{10}	2	C_{m20}	0
	L_{e1}	0.45	L_2	8.6	R_4	4.5	C_{m3}	4	L_{e10}	2.7	C_{m30}	0
	C_{e1}	0.56	R_3	2.7	L_4	0.06	k_{L1}	0	C_{e10}	0.8	k_{L10}	0.16

The circuit in Fig. 6(a) is of Parallel-Series type, meaning that the capacitor C_P is parallel with the series LC circuit which is made up of L_S and C_S. And the resonant frequency of this inner series LC circuit locates between f_l and f_h so it will present capacitance at f_l and inductance at f_h, making it possible that C_1 is larger than C_2. Given C_1, C_2, f_l, f_h, and C_P, the inductance L_S and capacitance C_S can be found by

$$C_S = \frac{(C_1 - C_P)(C_P - C_2)\left(f_h^2 - f_l^2\right)}{(C_1 - C_P) f_l^2 + (C_P - C_2) f_h^2} \tag{1a}$$

$$L_S = \frac{C_1 - C_2}{4\pi^2 (C_1 - C_P)(C_P - C_2)\left(f_h^2 - f_l^2\right)}. \tag{1b}$$

Similarly, for the Series-Parallel type of composite capacitor shown in Fig. 6(b), given C_1, C_2, f_l, f_h, and C_S, the inductance C_P and capacitance L_P can be readily solved.

III. DEMONSTRATION EXAMPLE

At first, one pair of dual-band IFAs is decoupled using the proposed composite capacitors of parallel-series type, as is shown in Fig. 7. The values of f_l and f_h are 1.84 and 3.5 GHz. Using a similar method to the example in Part B of Section II, C_1 and C_2 can be found as 3.5 and 0.75 pF. In this design, C_P is selected to be 1.4 pF, so C_S and L_S can be readily found as 0.8 pF and 5.76 nH according to formulas (1a) and (1b). In the EM simulation, due to the unavoidable connecting pad and parasitic effect, the values of the three elements are fine-tuned, and the final values are 1.2 pF, 0.85 pF, and 4.9 nH for C_P, C_S, and L_S.

In the prototyped sample, the soldering values of these three elements are 1.0 pF, 0.9 pF, and 5.1 nH. And Fig. 8 shows the top and bottom sides of the fabricated prototype. The soldered components of 1.0 pF, 0.9 pF, and 5.1 nH are high-Q series of

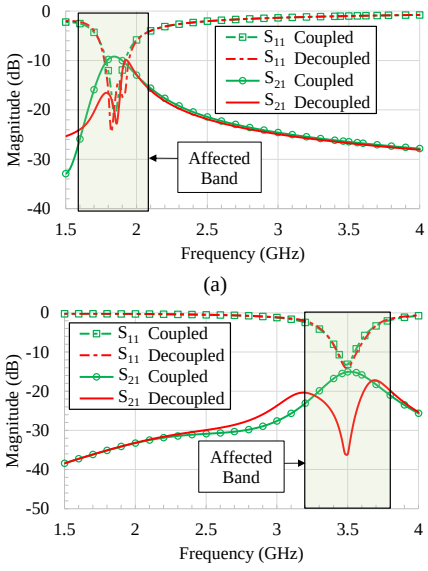

Fig. 5. Comparison of circuit simulated results between the coupled and decoupled cases. (a) Low band. (b) High band.

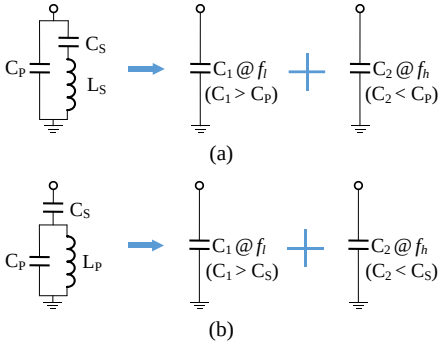

Fig. 6. Two circuit topologies of composite capacitors for the proposed dual-band decoupling scheme. (a) Parallel-Series type. (b) Series-Parallel type.

Murata to reduce undesired loss, and the total occupied size of the decoupling structure is only about 5 × 3 mm^2.

It is seen from Fig. 9 that the simulated and measured results agree well with each other. The results show that the isolation at the lower center frequency of 1.84 GHz is improved from about 9 dB to better than 20 dB, and from 13 to 28 dB at 3.5 GHz. In both frequency bands, the matching results are also improved as compared to those of the coupled counterpart.

It is found from Fig. 10 that the average total efficiency throughout the lower band (1.8 – 1.88 GHz) is improved from 62 % to 66 %, and from 50 % to 62 % for the higher band. The envelope correlation coefficient (ECC) is calculated using the measured far-field electric fields. As is shown in Fig. 10, the

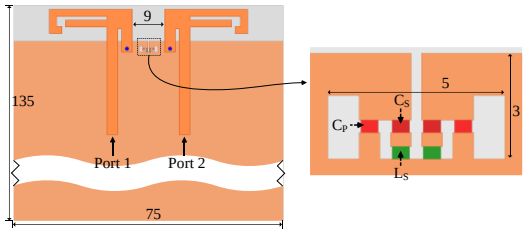

Fig. 7. Antenna geometry of the demonstrational example using proposed Parallel-Series type composite capacitors.

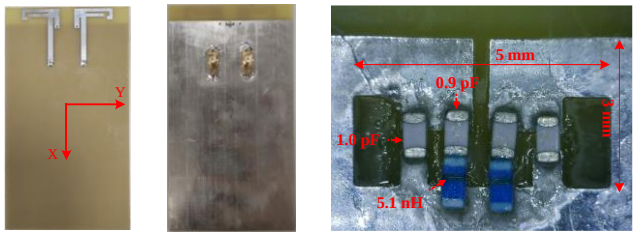

Fig. 8. Photos of the decoupled antennas. (a) Top side. (b) Bottom side. (c) Zoom-in view of the composite capacitors on the bottom side.

ECCs are reduced significantly after decoupling, from 0.26 to 0.046 in the low band and from 0.27 to 0.064 in the high band, indicating a lower spatial correlation.

A comprehensive comparison of the proposed dual-band decoupling method and the prior works is conducted in Table II. It is observed that the proposed method is based on the inherent frequency selectivity of the decoupling structure, and the design in the two bands is naturally independent of each other. Furthermore, the required footprint for the decoupling structure is the smallest, which is highly attractive to terminal MIMO antenna applications. And the achieved worst isolations within the desired bands are comparable with the prior works.

And the three components in the proposed composite circuit can be replaced using corresponding varactors or tunable switches to achieve frequency tuning to some extent. In particular, C_P mainly tunes the high band while C_S mainly tunes the low band, and L_S, and L_S can adjust the two bands simultaneously. Therefore, one can design a tunable circuit by replacing the elements with the corresponding tunable device according to these frequency control guidelines. And it should be noted that this reconfigurable capability is limited within a narrow band, which is mainly resulted from the matching degradation with a too-large tuning shift. And the simulated radiation efficiency with different component losses of the three elements is studied. It is found that the simulated radiation efficiency decrease with the component loss. Quantitatively, the radiation efficiency will decrease by about 2 % with a 0.1 Ω increase in the component loss.

To justify the generality, another example using series-parallel composite capacitors is further studied. And the working bands are tuned as 2.11 – 2.17 GHz (5G N1 band) and 3.4 – 3.6 GHz (5G N78 band) by tuning the length of the longer arm, as the antenna geometry and dimension shown in Fig. 11. To calculate the three element values of the composite capacitor, the values of f_l, f_h, C_1 and C_2 can be first found as 2.14 GHz, 3.5 GHz, 2.85 pF, and 0.8 pF. Similar to the above

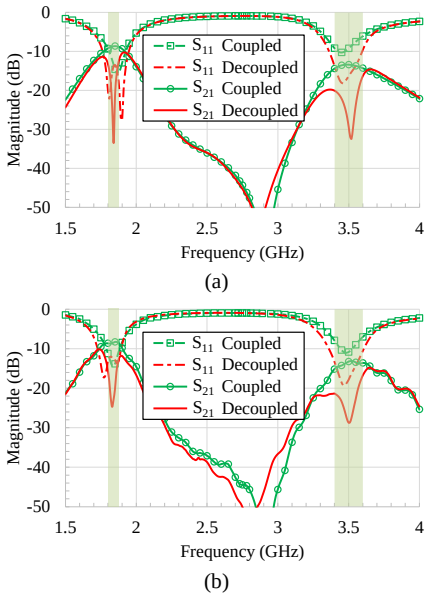

Fig. 9. Simulated and measured S-parameters of the demonstrational example. (a) Simulated. (b) Measured.

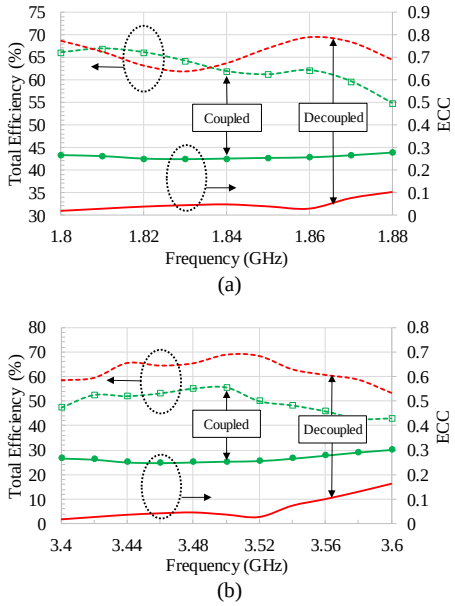

Fig. 10. Measured total efficiencies and calculated ECCs of the coupled and decoupled IFAs. (a) In the low band. (b) In the high band.

first example, C_S is selected as 1.25 pF, so C_P and L_P can be readily found as 4.88 pF and 0.78 nH.

The simulated S-parameters of the coupled and decoupled IFAs are compared in Fig. 12. It is found that the isolation at 2.14 GHz is improved from 7.8 to 23 dB after decoupling and from 11.6 to 26 dB at 3.5 GHz.

IV. Conclusion

An independently-controlled dual-band decoupling technique based on inherent frequency selectivity is presented in this paper. The working mechanism of the decoupling scheme is revealed by studying a concise equivalent circuit model. The circuit model reveals that the decoupling structure

TABLE II

COMPARISON OF STATE-OF-THE-ART DUAL-BAND DECOUPLING METHODS

Ref.	Bands (GHz)	Achieved Isolation (dB)	Independent Control	Size (mm^2)
[10][2017]	2.4 – 2.484 / 5.25 – 5.9	20.3 / 26.7	No	18.6 × 10
[14][2017]	2.4 – 2.5 / 5.7 – 5.9	15 / 20	No	43 × 10
[15][2018]	2.0 – 2.1 / 4.8 – 4.9	19 / 17	No	30 × 14
[16][2022]	2.4 – 2.484 / 5.15 – 5.875	20 / 20	No	42.2 × 11
[17][2020]	1.95 – 2.05 / 3.65 – 3.75	20 / 15	No	41 × 42.4
Proposed	1.8 – 1.88 / 3.4 – 3.6	15 / 18	Yes	5 × 3

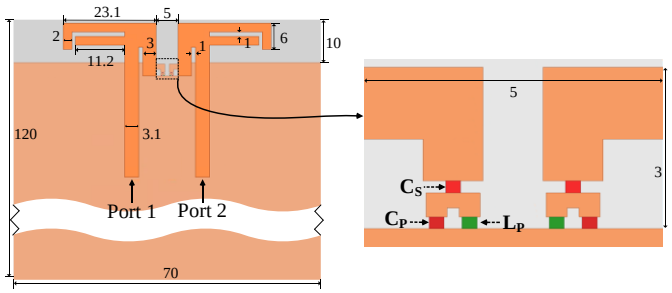

Fig. 11. Antenna geometry of the second example using proposed Series-Parallel type composite capacitors.

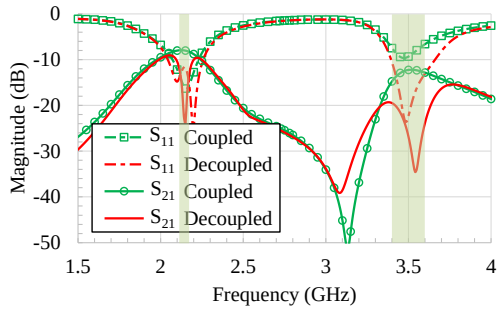

Fig. 12. Simulated S-Parameters of the second example.

is equivalent to a coupled series-resonant circuit, which has an independently controlled decoupling effect. And two composite capacitor circuits are proposed to further reduce the size of the decoupling structure. Two demonstrative examples are presented using the proposed composite capacitor circuits. The results show that the performances of a MIMO antenna array in the two bands, such as port isolation, impedance matching, total efficiency, and ECC are well improved after using the proposed dual-band decoupling scheme.

ACKNOWLEDGMENT

The authors would like to express their deep appreciation to Prof. Ke-Li Wu at The Chinese University of Hong Kong for his valuable and inspirational discussion and suggestions.

REFERENCES

[1] X. Chen, S. Zhang, and Q. Li, "A review of mutual coupling in MIMO systems," *IEEE Access*, vol. 6, pp. 24706–24719, 2018.

[2] F. M. Barradas, P. M. Tomé, J. M. Gomes, T. R. Cunha, P. M. Cabral, and J. C. Pedro, "Power, linearity, and efficiency prediction for MIMO arrays with antenna coupling," *IEEE Trans. Microw. Theory Techn.*, vol. 65, no. 12, pp. 5284–5297, Dec. 2017.

[3] C.-D. Xue, X. Y. Zhang, Y. F. Cao, Z. Hou, and C. F. Ding, "MIMO antenna using hybrid electric and magnetic coupling for isolation enhancement," *IEEE Trans. Antennas Propag.*, vol. 65, no. 10, pp.5162–5170, Oct. 2017.

[4] B. K. Lau and J. B. Andersen, "Simple and efficient decoupling of compact arrays with parasitic scatterers," *IEEE Trans. Antennas Propag.*, vol. 60, no. 2, pp. 464–472, Feb. 2012.

[5] C. Deng, D. Liu, and X. Lv, "Tightly arranged four-element MIMO antennas for 5G mobile terminals," *IEEE Trans. Antennas Propag.*, vol. 67, no. 10, pp. 6353–6361, Oct. 2019.

[6] J.-F Li, Q.-X. Chu, and T.-G. Huang, "A compact wideband MIMO antenna with two novel bent slits," *IEEE Trans. Antennas Propag.*, vol. 60, no. 2, pp. 482-489, Feb. 2012.

[7] L. Zhao, Y. He, G. Zhao, X. Chen, G. -L. Huang, and W. Lin, "Scanning Angle Extension of a Millimeter Wave Antenna Array using Electromagnetic Band Gap Ground," *IEEE Trans. Antennas Propag.*, vol. 70, no. 8, pp. 7264–7269, Aug. 2022.

[8] L. Sun, Y. Li, and Z. Zhang, "Wideband integrated quad-element MIMO antennas based on complementary antenna pairs for 5G smartphones," *IEEE Trans. Antennas Propag.*, vol. 69, no. 8, pp. 4466–4474, Aug. 2021.

[9] S. Zhang, B. K. Lau, Y. Tan, Z. Ying, and S. He, "Mutual coupling reduction of two PIFAs with a T-shape slot impedance transformer for MIMO mobile terminals," *IEEE Trans. Antennas Propag.*, vol. 60, no. 3, pp. 1521–1531, Mar. 2012.

[10] J.-H. Xun, L.-F. Shi, W.-R. Liu, G.-X. Liu, and S. Chen, "Compact dual-band decoupling structure for improving mutual coupling of closely placed PIFAs," *IEEE Antennas Wireless Propag. Lett.*, vol. 16, pp. 1985–1989, 2017.

[11] X. Tang, K. Mouthaan, and J. C. Coetzee, "Dual-band decoupling and matching network design for very closely spaced antennas," in *Proc. Eur. Microw. Conf.*, 2012, pp. 49–52.

[12] F. Liu, J. Guo, L. Zhao, G. Huang, Y. Li, and Y. Yin, "Dual-band metasurface-based decoupling method for two closely packed dual-band antennas," *IEEE Trans. Antennas Propag.*, vol. 68, no. 1, pp. 552–557, Jan. 2020.

[13] K.-C. Lin, C.-H. Wu, C.-H. Lai, and T.-G. Ma, "Novel dual-band decoupling network for two-element closely spaced array using synthesized microstrip lines," *IEEE Trans. Antennas Propag.*, vol. 60, no. 11, pp. 5118–5128, Nov. 2012.

[14] J. Sui and K.-L. Wu, "A general T-stub circuit for decoupling of two dual-band antennas," *IEEE Trans. Microw. Theory Techn.*, vol. 65, no. 6, pp. 2111–2121, Jun. 2017.

[15] Y.-F. Cheng and K.-K. M. Cheng, "A novel dual-band decoupling and matching technique for asymmetric antenna arrays," *IEEE Trans. Microw. Theory Techn.*, vol. 66, no. 5, pp. 2080–2089, May. 2018.

[16] M. Li, Y. Zhang, D. Wu, K. L. Yeung, L. Jiang, and R. Murch, "Decoupling and matching network for dual-band MIMO antennas," *IEEE Trans. Antennas Propag.*, vol. 70, no. 3, pp. 1764–1775, Mar. 2022.

[17] K.-D. Xu, H. Luyen, and N. Behdad, "A decoupling and matching network design for single- and dual-band two-element antenna arrays," *IEEE Trans. Microw. Theory Techn.*, vol. 68, no. 9, pp. 3986–3999, Sep. 2020.

[18] J. Sui, Y. Dou, X. Mei, and K.-L. Wu, "Self-curing decoupling technique for MIMO antenna arrays in mobile terminals," *IEEE Trans. Antennas Propag.*, vol. 68, no. 2, pp. 838-849, Feb. 2020.

[19] J. Sui, C. Huang, and Y.-F. Cheng, "Multi-element fully-decoupled inverted-F antennas for mobile terminals," *IEEE Trans. Antennas Propag.*, vol. 70, no. 11, pp. 10076–10085, Nov. 2022.